JOURNAL OF APPLIED POLYMER SCIENCE VOL. 15, PP. 2487–2512 (1971)

Relationships Between Mechanical Properties and Relaxation Processes in Polymers. Nylon 6

C. GARBUGLIO, G. AJROLDI, T. CASIRAGHI, and G. VITTADINI,
Montecatini Edison, S.p.A., Centro Ricerche Bollate, 20021 Bollate (Milano), Italy

Synopsis

The dynamic-mechanical properties as a function of temperature and frequency were measured for five samples of polycaprolactam (nylon 6) containing different amounts of hydrosoluble products. Low- and high-speed tensile properties and Izod impact strength were determined between −190° and 100°C for the same samples by using autographic methods. The influence of the mechanical relaxation processes on moduli, yield strength σ_y, yield strain ϵ_y, tough-brittle transition temperature, elongation at break ϵ_R, and tensile and Izod fracture energies was investigated. It has been found that some mechanical properties, such as modulus and yield properties, can be directly related to specific relaxation phenomena, whereas as far as other properties, such as the ultimate properties, are concerned, the existing correlation can be concealed by the interference of purely mechanical phenomena which depend on the testing technique used, the testing conditions, and the previous history of the material.

INTRODUCTION

Several papers dealing with the problem of the correlations between dynamic-mechanical properties and impact properties of plastic materials[1−3] have appeared in the literature. A comprehensive review on this topic has recently been published by Boyer[4] who emphasized the controversial nature of the problem. Besides the obvious difficulties in relating the results obtained by experimental methods that are widely different in regard to test conditions, strain rates, and geometric characteristics, the ultimate properties cannot, in general, be directly related to molecular relaxation processes, as Vincent has pointed out for the tough-brittle transition.[5]

In a previous work,[6] the influence of the hydrosoluble products on the dynamic-mechanical properties of polycaprolactam has been investigated and some physical properties have been determined at 23°C. A qualitative relationship was found between the logarithmic decrement Δ and the Izod impact strength at room temperature. In the present work, a comprehensive approach for relating the mechanical behavior with molecular relaxation processes has been attempted for polycaprolactam through a detailed analysis of the different parameters that influence the mechanical and the

© 1971 by John Wiley & Sons, Inc.

dynamic-mechanical behavior studied in a wide range of temperatures and frequencies.

EXPERIMENTAL

Materials

The polycaprolactam used in this work was obtained by means of hydrolytic polymerization.[7] The raw material had a number-average molecular weight $\bar{M}_n$ = 16,000 and an hydrosoluble content of about 8%. Four portions were water extracted for different periods of time in order to obtain different hydrosoluble contents. The five materials, before molding, were dried so as the water content was ca 0.1%. The specimens were obtained by injection molding at a mold temperature of 80°C. The specimens for tensile and dynamic-mechanical measurements at low frequency were cut from disks of 1.1-mm thickness and 105-mm diameter. The specimens for the dynamic-mechanical tests, carried out by means of the Brüel and Kjaer apparatus, had the dimensions of $^1/_8 \times {}^1/_2 \times 10$ in. The same specimens were used for the Izod impact test. The hydrosoluble content was determined by extracting with water[8] the molded specimens, and the results are reported in Table I. Finally, all the specimens were oven conditioned in vacuo at 60°C for 48 hr and stored in vacuo over $CaCl_2$ at 23°C.

TABLE I
Characteristics of Polycaprolactam Samples

Sample	Hydrosoluble content, wt-%		Specimen density, g/cm³	
	Before molding	After molding	0.1-cm thick	0.35-cm thick
A	0.6	1.5	1.1244	1.1305
B	1.6	3.4	1.1249	1.1311
C	3.2	4.5	1.1280	1.1348
D	5.6	7.0	1.1308	1.1371
E	8.0	8.8	1.1316	1.1359

Tensile Measurements

Low-speed measurements were performed by an Instron tensile tester at a speed of 0.0083 cm/sec and using the Instron environmental test chamber between −60° and 100°C. Tests at lower temperatures were carried out by immersing specimen and jaws in a cooling bath (liquid N_2, or liquid N_2 and freon 22 or 12). The freons used were freshly prepared because it was observed that freon stored for a long time develops stress cracking phenomena. High-speed tensile tests were carried out by means of a modified impact pendulum which enables the recording of load-time curves.[9] The specimens were conditioned on the apparatus by cooling or heating with special pliers made of heavy copper masses, which were,

previously immersed into a thermostated bath. The temperature of each specimen was controlled by a thermocouple.

Type S specimens (ASTM D1822) were obtained from the aforementioned disks through accurate milling. Microscope and polarized light observations were carried out in order to check the accuracy of the milling and the roughness of the surfaces.

Some tensile measurements were carried out on specimens cut parallel and perpendicular to the flow direction. Since no orientation effects were found, specimens cut parallel to the flow direction were used throughout the work.

The gauge length of 1.5 cm was taken as L_0; this assumption, using S-type specimens, is somewhat incorrect but does not lead to serious errors. The apparent strain rates $\dot{\epsilon}$ calculated on this basis are 230 sec^{-1} and 0.0055 sec^{-1} for high- and low-speed tests, respectively. Instron data were corrected for the deformation of the system.

Izod Impact Strength

A standard pendulum equipped with a strain gauge load cell was used.

Notched specimens ASTM D256-56 $^1/_8 \times {}^1/_2 \times 2.5$ in. were obtained from molded bars. The clamping force, determined by a load cell, was fixed at 30 kg/cm^2. The specimens were conditioned by immersion in thermostated baths. The time required for transferring clamping and breaking the specimens was about 5 sec; the temperature, measured immediately before the break, was considered to be the test temperature.

Dynamic-Mechanical Testing

The dependence of the dynamic-mechanical properties on the frequency was investigated either by means of a free oscillation torsion pendulum[10] in the range of about 2 Hz or by a Brüel and Kjaer Complex Modulus Apparatus[11] in the frequency range between 40 and 1000 Hz. The specimen dimensions were $10 \times 1 \times 0.1$ cm and $^1/_8 \times {}^1/_2 \times 10$ in. for the two apparatuses, respectively. The storage shear modulus G', the storage modulus E', and tan δ were derived by well-known equations.[12]

Density

The density was determined by a gradient column according to ASTM D1505-60T method at 23°C. The liquids employed were toluene and carbon tetrachloride. The results are reported in Table I.

Electron Micrographs

The fracture surfaces of some Izod specimens were observed by means of an electron-scanning microscope, Cambridge Mark II. The specimens were plated in vacuo with a gold–platinum alloy.

EXPERIMENTAL RESULTS

The low-frequency dynamic-mechanical properties, log G′ and log tan δ, for samples A and E are plotted in Figure 1 as a function of temperature. The storage Young modulus E' and tan δ obtained by the Brüel and Kjaer apparatus are plotted on a semilogarithmic scale in Figure 2 for the same samples.

The stress–strain (σ–ϵ) curves, determined between −170° and +185°C from tensile impact tests,[9] are plotted in Figures 3 and 4 for samples A and E, respectively.

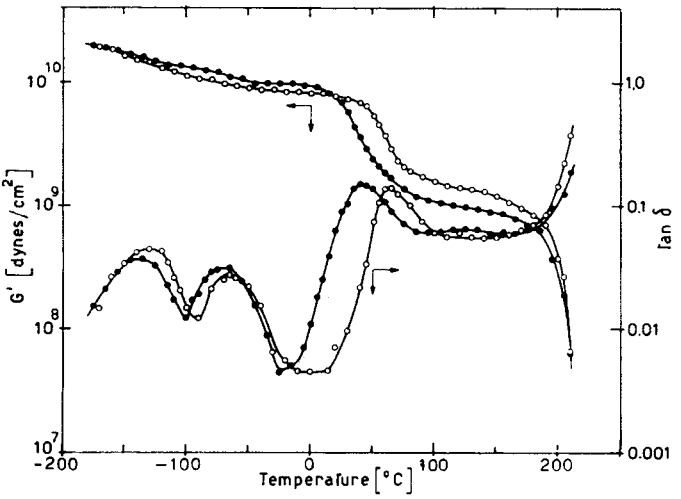

Fig. 1. Effect of hydrosoluble content on the low-frequency (ca. 2 Hz) dynamic-mechanical properties of polycaprolactam: (O) sample A; (●) sample E.

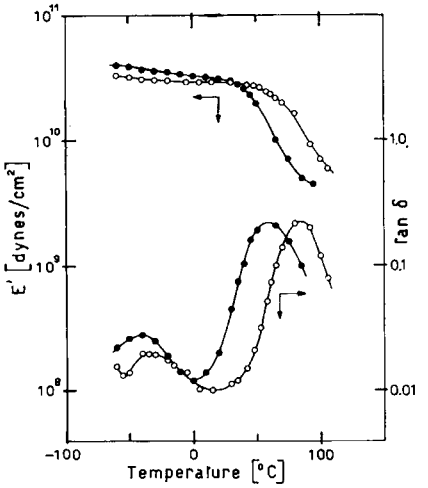

Fig. 2. Effect of hydrosoluble content on dynamic-mechanical properties of polycaprolactam measured at 200 Hz: (O) sample A; (●) sample E.

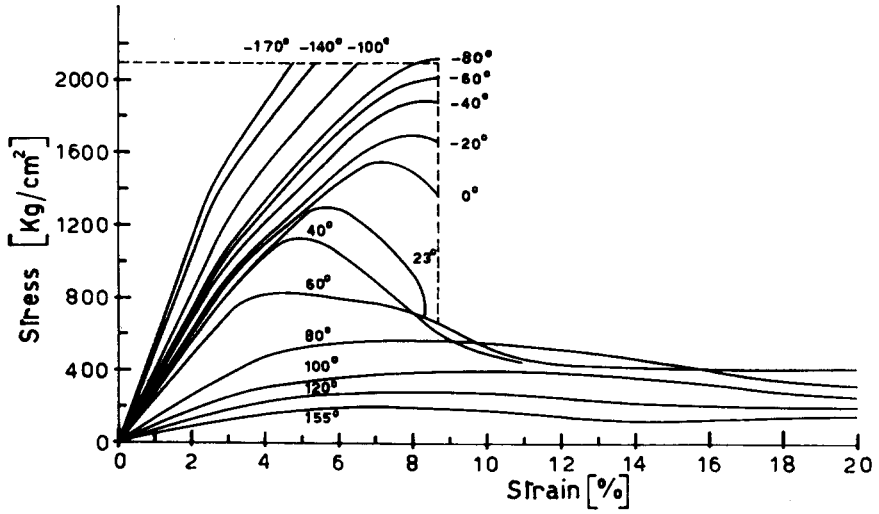

Fig. 3. Stress–strain curves for sample A measured at $\dot{\epsilon} = 230$ sec^{-1} and at several temperatures. Dotted lines identify the box (see text).

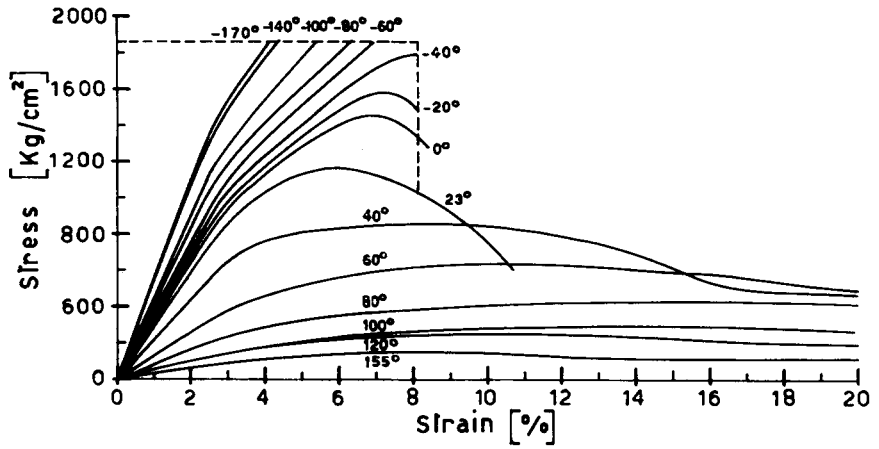

Fig. 4. Stress–strain curves for sample E measured at $\dot{\epsilon} = 230$ sec^{-1} and at several temperatures. Dotted lines identify the box (see text).

Some high-speed tensile-test oscillographic recordings are shown in Figure 5. The low-speed stress–strain curves σ–ϵ, measured between $-195°$ and $+100°$C with the Instron dynamometer, for samples A and E are plotted in Figures 6 and 7, respectively.

The isochronous relaxation Young modulus E (t = const.) was calculated from the σ–ϵ curves as $d\sigma/d\epsilon$ at 1% elongation, and the time was calculated at $t = \epsilon/\dot{\epsilon}$.[13] The E-versus-T curves obtained at $t = 4.35 \times 10^{-5}$ sec ($\dot{\epsilon} = 230$ sec^{-1}) and at $t = 1.8$ sec ($\dot{\epsilon} = 0.0055$ sec^{-1}) are plotted in Figure 8 for samples A and E. The yield stress σ_y, the yield strain ϵ_y, the apparent

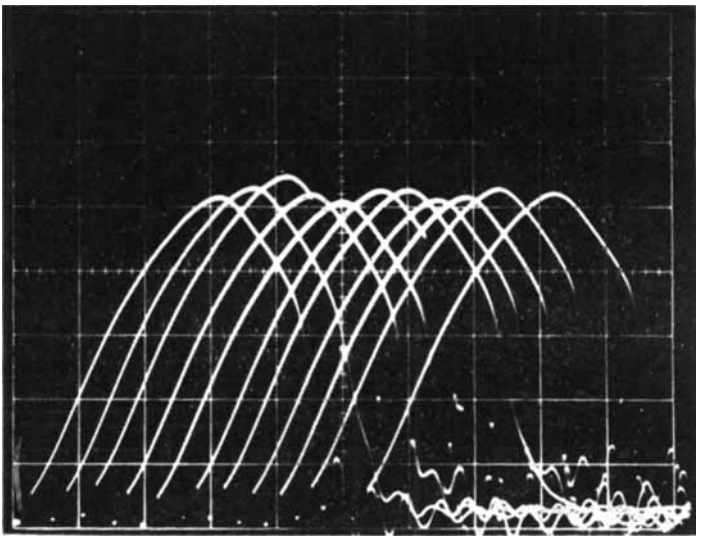

Fig. 5. Oscillographic record of the high-speed tensile test of 11 specimens of sample A measured at 23°C: x-axis: 0.1 msec/div; y-axis: 3 mV/div.

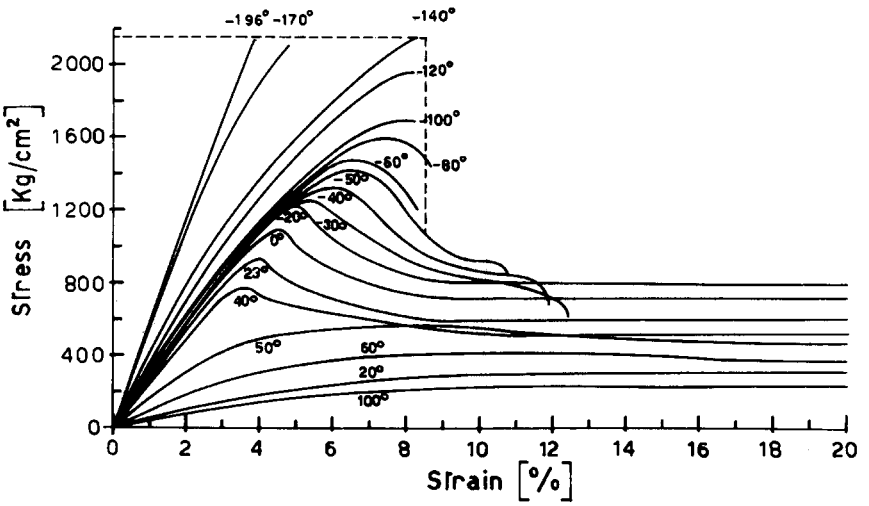

Fig. 6. Stress–strain curves for sample A measured at $\dot{\epsilon} = 5.5 \times 10^{-3}\,\text{sec}^{-1}$ and at several temperatures. Dotted lines identify the box (see text).

elongation at break ϵ_R, and the fracture energy were also measured from the $\sigma-\epsilon$ curves.

Some oscillographic recordings obtained by the Izod impact test are shown in Figure 9. From the load-time curves so obtained, the secant modulus, defined as the ratio between the stress (mV) and the time (msec) at break, was calculated and is plotted in Figure 10.

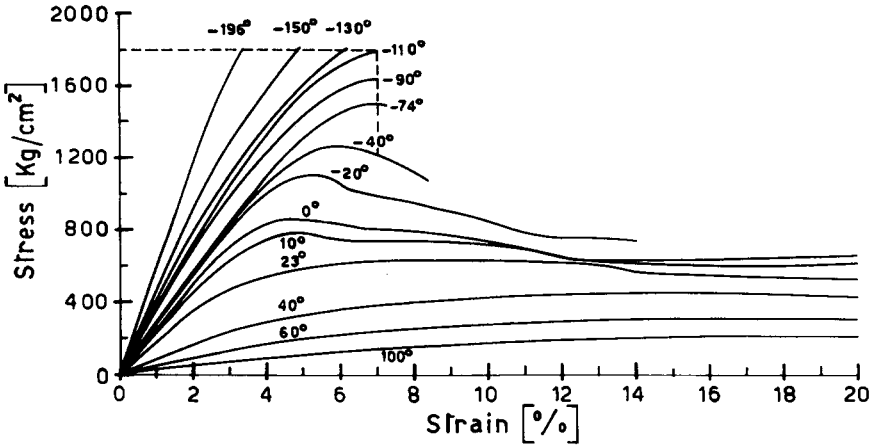

Fig. 7. Stress–strain curves for sample E measured at $\dot{\epsilon} = 5.5 \times 10^{-3}\,\mathrm{sec}^{-1}$ and at several temperatures. Dotted lines identify the box (see text).

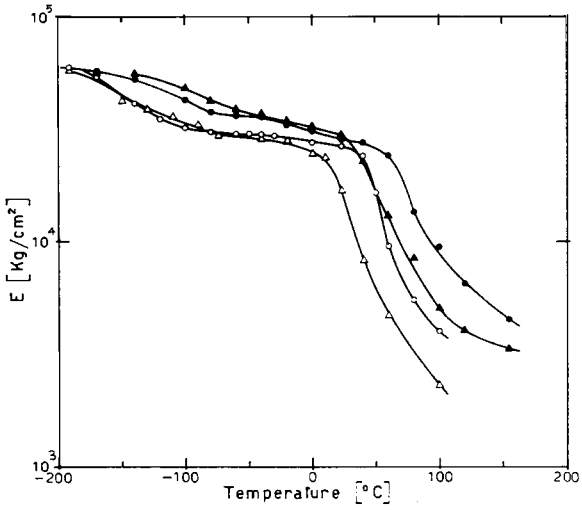

Fig. 8. Plot of the Young modulus E against temperature for samples A and E measured at two different times: $t = 4.35 \times 10^{-4}$ sec, (●) sample A; (▲) sample E. $t = 1.8$ sec, (○) sample A; (△) sample E.

DISCUSSION

Mechanical Relaxation Processes

As shown in Figure 1, the loss factor curves, measured at about 2 Hz, display three dispersion regions between −190°C and the melting temperature. These dispersions are found at about −140°C, −70°C, and 62°C, respectively. The γ-process, at −140°C, is related to an in-chain motion of 4 to 6 methylene groups.[14,15] The attribution of the β-maximum,

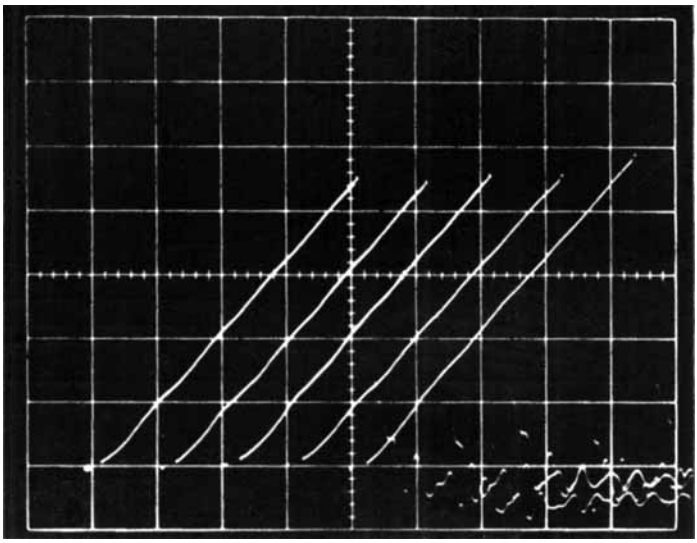

Fig. 9. Oscillographic recording of the Izod impact test of five specimens of sample A measured at 23°C: x-axis: 0.1 msec/div; y-axis: 5 mV/div.

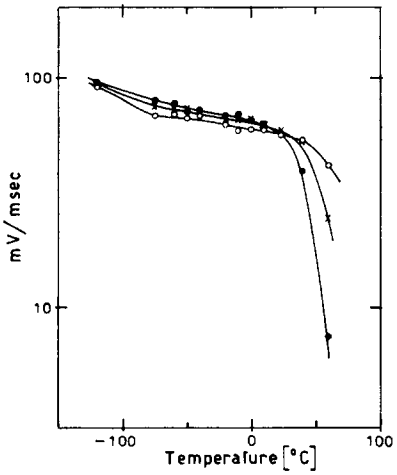

Fig. 10. mV/msec ratio, obtained from Izod stress–time curve, against temperature for samples A (O), C (x), and E (●).

which appears at −70°C, to a molecular relaxation process, is still controversial; according to Illers,[16] it could be related to a side-chain-like motion of the hydrosoluble molecules linked to the main chain through hydrogen bonding. The α-maximum, at 62°C, is related to the glass transition of the amorphous regions of the polycaprolactam.[6,17]

The modulus decreases noticeably in the temperature range of the γ- and α-maxima, whereas it seems to be unaffected by the β-relaxation process.

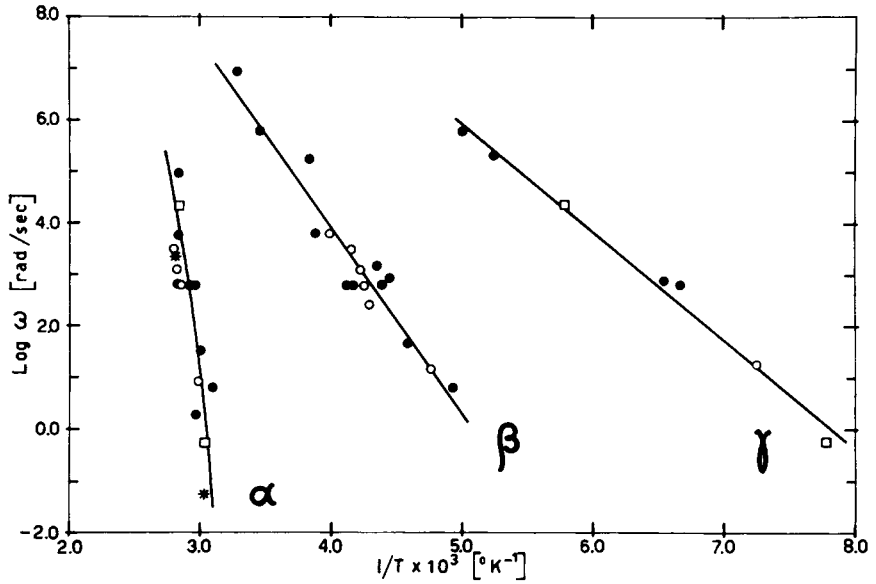

Fig. 11. Dependence of T_α, T_β, and T_γ on the circular frequency ω, from dynamic-mechanical properties (○); from tensile properties (□); from yield properties (x); literature data (●) (see refs. 16, 17, and 19).

The tan δ maxima are shifted toward lower temperature by increasing the hydrosoluble content which, in the case of the β- and γ-maxima, also affects their intensity as previously shown by us[6] and by other authors.[18] The shifting effect of the frequency on the β- and α-relaxation maxima is evident by comparison of the tan δ-versus-T curves obtained at ca. 2 Hz with those obtained at 200 Hz, which are plotted in Figures 1 and 2, respectively.

Similar effects can be noted in the isochronous relaxation modulus E (t = const.)-versus-T curves, obtained at two different strain rates, as shown in Figure 8. From these curves the approximate locations of the α- and γ-maxima were obtained from the maxima of the derivative $-d\ln E/dT$, which was calculated by means of the least-squares method of derivation.[19] This approximate method to estimate T_α and T_γ was checked by deriving some G'-versus-T curves; a good agreement between the tan δ maxima and the $-d\ln G'/dT$ maxima was found.

The T_α, T_β, and T_γ values, obtained at various frequencies for sample A, were plotted, in Figure 11, as $\log \omega$ (or $\log \omega = \log 1/t$ in the case of data obtained from the tensile moduli curves) versus $1/T$ together with the literature data.[17,18,20] A good agreement was found, and the values of $\Delta E(\gamma) = 9.6$ and $\Delta E(\beta) = 16.5$ Kcal/mole for the activation energies of of the γ- and β-processes were calculated by the least-squares method. The dependence of the α-relaxation maximum on the temperature is described by the well-known WLF equation.[21] Some scattered points are observed,

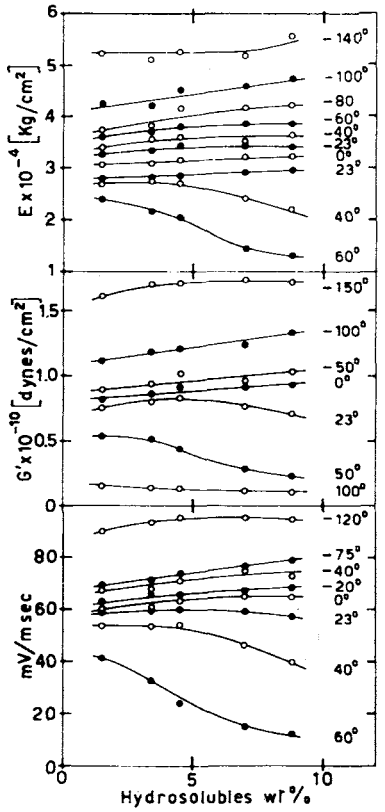

Fig. 12. Dependence on hydrosoluble content, at several temperatures, of: (a) tensile modulus E, (b) storage shear modulus G', and (c) mV/msec ratio obtained from the Izod impact test.

but it should be pointed out that the water or the hydrosoluble content was unknown for some of the data taken from the literature. Furthermore, T_α is greatly influenced by the amount of crystallinity and by the crystalline form.[22,23]

In Figure 12, the dependence of the moduli on the hydrosoluble content at different temperatures is reported; it can be seen that the moduli at low temperatures have higher values for those samples having the highest hydrosoluble content. Such results agree with our previous findings[6] and with those reported by other authors.[16,18,24] The increase in modulus should be attributed to the closer packing of the macromolecular chains; as a matter of fact, also the density increases by increasing the hydrosoluble content (see Table I).

Tensile Properties

A detailed analysis of the σ–ϵ or σ–t curves provides some information about the relative contribution of the stored and dissipated energy during

the breaking process; their ratio varying with temperature and strain rate, as shown in Figures 3, 4, 6, and 7. The presence of three different zones of mechanical behavior, indicated as rigid, plastoelastic, and rubbery by Chatain and Dubois,[25] can also be easily observed. Indeed, the curves reported in Figure 3, obtained in the range −170° to 23°C, can be inscribed in a box (Fig. 3, dotted line). The same result can also be obtained for the curves reported in Figures 4, 6, and 7, where the temperature ranges are shifted because of different hydrosoluble content or strain rate.

The upper boundary (first zone) is characterized by a nearly constant failure strength, and the so-called "brittle" behavior is always found; the energy at break is mainly a stored strain energy. The right-side boundary of the box (second zone) is characterized by a nearly constant apparent strain at break. In this zone, some of the curves show the yield phenomenon, and the energy dissipated through a plastic deformation begins to rise markedly with temperature. However, a large amount of energy is stored as elastic energy, which is mainly responsible for the propagation of cracks until complete fracture occurs. It must be pointed out that in this second zone, two mechanisms are undoubtedly present[26] before necking: one is related to the process of plastic deformation and the other, to failure processes. The simultaneity of these mechanisms leads to a mechanical instability[27] caused concurrently by the catastrophic yielding of the structure, by a temperature increase localized in a small volume, and by elastic restoring forces in the portion of the specimen that has not yielded. The behavior at break seems to be more dependent on the mechanical equilibrium than on the viscoelastic processes, since the strain at rupture is independent of temperature.

The third zone is characterized by an increasing strain at rupture and by a decrease in tensile strength; the energy is mainly dissipated via large plastic deformations. The lower end of this zone is always about 50°C lower than the main transition range and is shifted along the temperature scale both by the hydrosoluble content and by strain rate. A comparison between the tensile data obtained at high and low speed (see Figs. 3 and 6) shows that the values of the boundaries of the box seem to be quite independent of strain rate; this fact points out that the failure envelopes which are well known for elastomeric materials,[28] are also present in thermoplasti polymers.

Yield Properties

The yield strength σ_y and the yield strain ϵ_y, measured at two different strain rates, are plotted against temperature in Figures 13 and 14, respectively, for samples A and E.

Starting from the lowest temperature at which the yielding process appears, the slope of the σ_y–T curves decreases up to the α-transition range, where it increases suddenly. At temperatures higher than T_α, the yielding process is still present, and the value of σ_y decreases slowly with increasing temperature. Even though the yield point is not evident in the enlarged

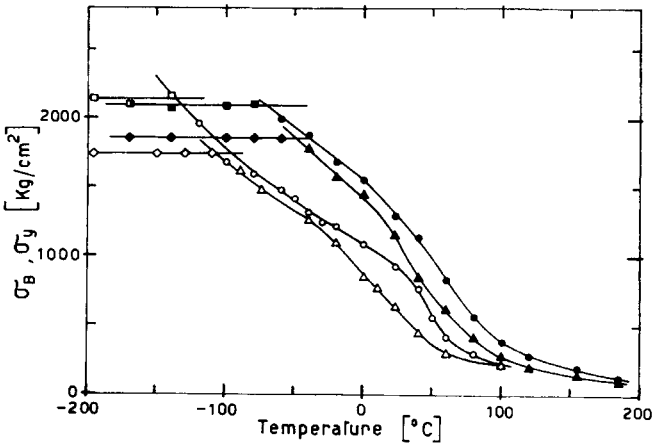

Fig. 13. Dependence of brittle strength σ_B and yield stress σ_y on temperature and strain rate for samples A and E. Sample A at $\dot{\epsilon} = 230\ \text{sec}^{-1}$: (■) σ_B; (●) σ_y. Sample A at $\dot{\epsilon} = 5.5 \times 10^{-3}\ \text{sec}^{-1}$: (□) σ_B; (○) σ_y. Sample E at $\dot{\epsilon} = 230\ \text{sec}^{-1}$: (◆) σ_B; (▲) σ_y. Sampoe E at $\dot{\epsilon} = 5.5 \times 10^{-3}\ \text{sec}^{-1}$: (◇) σ_B; (△) σ_y.

scale used in Figures 3, 4, 6, and 7 for $T > T_\alpha$, it can easily be observed in the original recorded stress–strain curves. As an example, the oscillographic recording of a tensile impact test carried out at 155°C for sample A is reported in Figure 15.

It is well known that for amorphous polymers, σ_y and ϵ_y should disappear at temperatures above T_α; our experimental results point out that the nonzero value of σ_y for $T > T_\alpha$ is connected with the yielding of the crystalline phase of the material. A similar behavior was found by Roetling in the case of polypropylene.[29]

By increasing the strain rate, the σ_y–T curves are shifted toward higher temperatures, thus showing that the yielding process is an activated process. The influence of strain rate on the yield properties was theoretically predicted by some authors[29–32] by assuming that the yield is an activated process and by applying to it the Ree-Eyring theory.[33] Moreover, in some cases it has been found that the activation energy of the flow units of the Eyring model is identical to that of the dynamic-mechanical relaxation processes and that the number of flow units and of the relaxation processes is the same.

Thus, in the present case we hypothesize that the yielding process can be described by a four-flow-unit Eyring model, three of which units belong to the amorphous phase and are connected with the γ-, β-, and α-relaxation processes; the fourth, as shown above, is connected with the yielding of the crystalline phase.

For an Eyring model composed of only one flow unit and in the special case where

$$\sinh^{-1}[\tau_0\dot{\epsilon}\exp(\Delta E/RT)] = \ln 2\tau_0\dot{\epsilon} + \Delta E/RT \qquad (1)$$

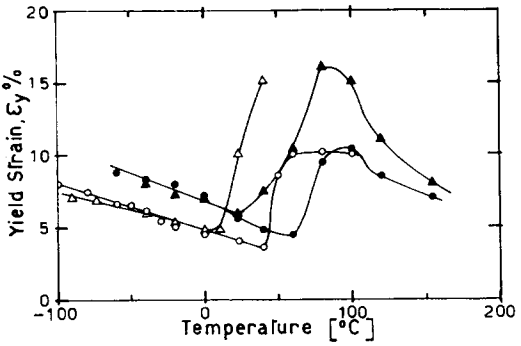

Fig. 14. Dependence of yield strain ϵ_y on temperature and strain rate for samples A and E: $\dot{\epsilon} = 230\,\text{sec}^{-1}$: (●) sample A; (■) sample E·$\dot{\epsilon} = 5.5 \times 10^{-3}\,\text{sec}^{-1}$: (○) sample A; (□) sample E.

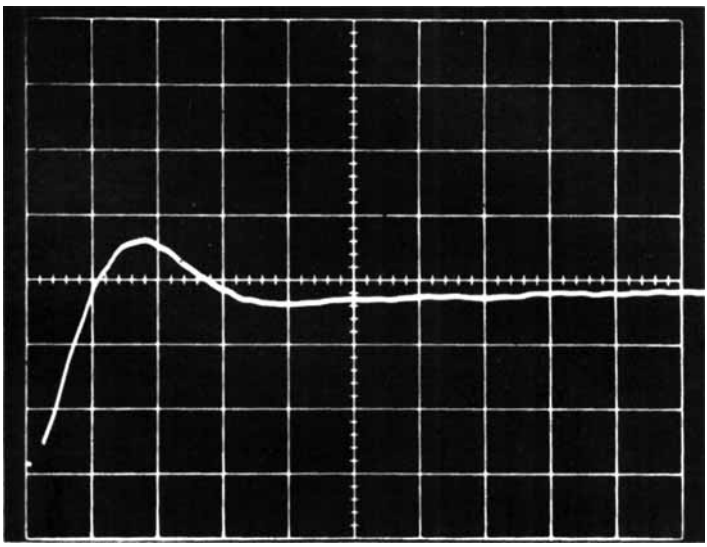

Fig. 15. Oscillographic recording of high speed tensile test for sample A at 155°C showing the yield point: x-axis, 0.2 msec/div; y-axis, 1 mV/div.

where τ_0 is the relaxation time and ΔE is the apparent activation energy, the dependence of σ_y on temperature is described by a straight line, as in the case of the σ_y/T-versus-$\dot{\epsilon}$ plots considered by other authors.[29–32] Deviations from such a trend are observed in the proximity on the α-transition range, where the influence of the free volume is superimposed on the activated rate process: σ_y tends rapidly toward zero and an inflexion point is observed in the T_α range.[31] On this basis the existence of a flow unit connected with the α-relaxation process is evident from Figure 13; the location of the inflexion point on the temperature scale was determined by carrying out the derivative $-d\ln\,\sigma_y/dT$, as described previously for the moduli curves. The points obtained for sample A at the two strain rates

were plotted on the activation energy plot (Fig. 11) and were found to lie rather close to the WLF curve, which describes the dependence of the α-relaxation process on temperature. Such a result is in good agreement with those obtained by Bauwens et al.[31] for poly(vinyl chloride) and polycarbonate in the glass transition range.

When σ_y is dependent on more than one flow unit and eq. (1) holds for all the flow units, the trend of σ_y against temperature is represented by a straight line whose intercept and slope are the sum of the intercepts and slopes characteristics of the single flow units.

On the other hand, if for one of the flow units the argument of the $\sinh^{-1}$ tends toward zero, the σ_y-versus-T curve has the shape of two crossing straight lines, the slope of the straight line at low temperatures being higher than that at higher temperatures. This fact can be easily observed for sample A tested at $\dot{\epsilon} = 5.5 \times 10^{-3}$ sec^{-1} (Fig. 13). The slope increases at temperatures lower than -80°C, showing the presence of a second flow unit which can be related to the γ-relaxation process. Experimental data do not show evidence of a flow unit which can be related to the β-relaxation process. Dynamic-mechanical experiments have shown[6] that T_α and T_γ are lowered by increasing the hydrosoluble content; consequently, the σ_y–T curves are shifted toward lower temperatures.

The deformation at yield ϵ_y, as shown in Figure 14, decreases by increasing the temperature up to the T_α range; thereafter it increases suddenly. This increase should be attributed to the contribution of the crystalline phase, since it is well known that ϵ_y tends toward zero in the glass transition range for amorphous polymers.[32]

For a semicrystalline polymer, the yielding behavior in the T_α range can be roughly represented by a mechanical model composed of a St. Venant body[34] coupled in series with a spring; the spring simulates the mechanical behavior of the amorphous phase and the frictional forces represent the yield strength of the crystalline phase. If a force is progressively applied to this mechanical model, the spring elongates until the force reaches the value of the frictional forces. At this point, the mass begins to move, that is, the amorphous phase is strained until the yield stress of the crystalline phase is reached. The stiffness of the amorphous phase decreases rapidly in the T_α range with increasing temperature, so that ϵ_y increases. In the case of nylon 6, the ϵ_y–T maximum is shifted toward lower temperatures either by lowering the strain rate or by increasing the hydrosoluble content. The height of the ϵ_y peak at T_α is a function of the hydrosoluble concentration and increases with it, probably because of the plasticizing effect of the hydrosolubles on the amorphous phase.[6]

The Tough-Brittle Transition

The definition of the tough-brittle transition temperature, which is useful from a practical point of view, is based on the macroscopic observation of the stress–strain behavior of the material. However, it is not rigorously correct because the brittle failure of a polymer seems to be always coupled

with some plastic deformation, which can be easily detected by microscopic inspection of the failure surfaces. Usually the tensile behavior of a polymer is called brittle or tough when the yield point, defined as the point where $d\sigma/d\epsilon = 0$, is absent or present.[5] However, the assignment of a point to the brittle or tough behavior may be uncertain when the specimen breaks near the yield point. In the present case, the tough-brittle transition temperature was defined on the basis of the box previously found, and it was assumed to lie at the intersection of the upper and the right-side boundaries of the box. It was thus possible to classify unambiguously as brittle strength σ_B the maximum stress of the σ–ϵ curves crossing the upper boundary and as σ_y the maximum stress of the σ–ϵ curves crossing the lateral boundary, even in those cases where the slope $d\sigma/d\epsilon$ approaches zero without attaining it. The σ_B and σ_y points reported in Figure 13 were obtained by applying this criterion, and the temperature at the intersection of the σ_B and σ_y curves is obviously that of the intersection of the boundaries of the box (see Fig. 3).

The results plotted in Figure 13 show also the influence of the strain rate on the tough-brittle transition. For sample A at $\dot{\epsilon} = 0.0055$ sec^{-1}, it lies at about -138°C, and for $\dot{\epsilon} = 230$ sec^{-1}, at about -72°C.

The shift of the tough-brittle transition on the temperature scale is due to the dependence of the σ_y–T curves on strain rate, the σ_B–T curve being fairly independent of it. Moreover, the results obtained for sample E and plotted in the same figure show that, even though the σ_y–T curves, measured at the two given strain rates, are shifted as a whole toward lower temperatures by the presence of low molecular weight components, tough-brittle transition temperatures higher than those for sample A are obtained since the level of σ_B is lower.

All this indicates that the tough-brittle transition temperature, i.e., the temperature at which the σ_B–T and σ_y–T curves intersect, is determined both by the value of the brittle strength and its dependence on the temperature and by the dependence of the yield strength on the temperature and

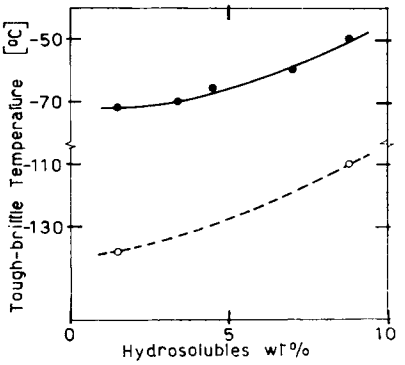

Fig. 16. Influence of hydrosoluble content on the tough-brittle transition temperature: (●) $\dot{\epsilon} = 230$ sec^{-1}; (○) $\dot{\epsilon} = 5.5 \times 10^{-3}$ sec^{-1}.

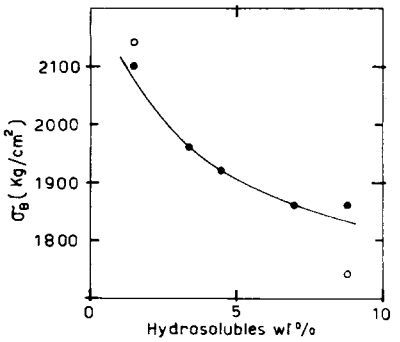

Fig. 17. Brittle strength σ_B plotted vs. hydrosoluble content (wt-%): (●) $\dot{\epsilon} = 230$ sec^{-1}; (○) $\dot{\epsilon} = 5.5 \times 10^{-3}$ sec^{-1}.

strain rate. That is, the tough-brittle transition depends on the concentration of defect loci in the specimen, which determines the level of σ_B, and on the activated relaxation processes, which determine the yielding behavior and therefore its activation energy.

It is thus clear that the tough-brittle transition temperature cannot be easily predicted. Only the yield behavior as a function of temperature and strain rate can be predicted on a molecular basis, whereas the dependence of σ_B on the molecular and morphologic structure and on the defect loci concentration is generally unknown.

As seen before, the presence of the hydrosolubles increases the tough-brittle transition temperature T_B of nylon 6 (see Fig. 16); this is related to the lowering of σ_B by increasing the hydrosoluble content (Fig. 17).

Ultimate Properties

In Figure 18, the apparent strain at break ϵ_R is plotted against the temperature on a semilogarithmic scale, for the low- and high-speed measurements for samples A and E. The curves have the same shape but are shifted along the temperature scale.

At low temperatures, ϵ_R increases smoothly, and a step in the curve is evident near the tough-brittle transition temperature; then it remains constant, according to the box defined before, until the α-transition range is reached; after that, it increases rapidly. Such behavior is well known for crosslinked rubbers,[35] and it has been shown recently by Retting for poly(vinyl chloride).[36] According to Bucknall,[37] the sudden increase in ϵ_R can be classified as a tough-tough transition. ϵ_R begins to increase about 50°C below the α-transition temperature; such behavior can be attributed to the influence of the free volume, which affects the physical properties of polymers only at temperatures above thermodynamic second-order transition temperature T_2.[32,38] The broad maximum in the α-transition range cannot be quantitatively discussed because of the heating of the sample at large strains. The dependence of ϵ_R on the hydrosoluble con-

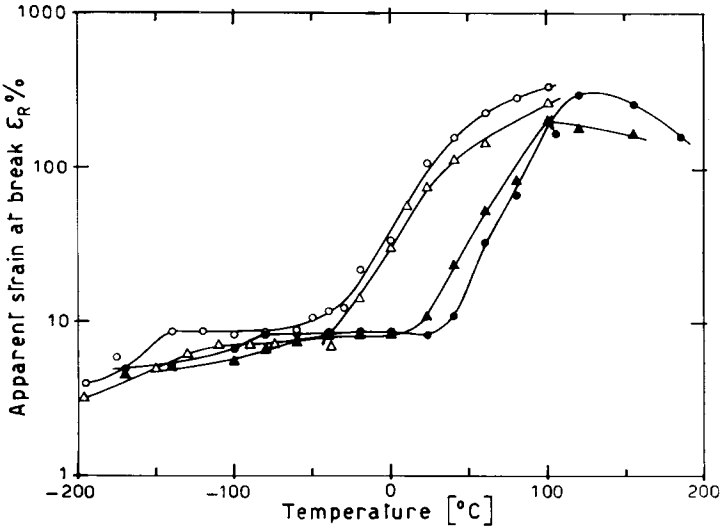

Fig. 18. Dependence of apparent strain at break ϵ_R on temperature and strain rate for samples A and E. $\dot{\epsilon} = 230$ sec^{-1}: (●) sample A; (▲) sample E. $\dot{\epsilon} = 5.5 \times 10^{-3}$ sec^{-1}: (○) sample A; (△) sample E.

tent and the strain rate is similar to that of the other properties discussed earlier.

Fracture Energy

The energy at rupture for samples A and E, measured at the two given strain rates, is plotted against temperature in Figure 19. Two maxima, which are dependent on strain rate and hydrosoluble content, are evident; the first one, which lies in the low-temperature range, appears at about the same temperature as the tough-brittle transition and the second one, near the α-transition range.

The low-temperature maximum can be explained by means of the stress–strain curves plots in Figures 3, 4, 6, and 7, which show that the area under the curves increases up to T_B and then decreases with increasing temperature because the apparent strain at rupture ϵ_R remains constant until the free volume becomes active. The maximum is frequency dependent, and its activation energy is the same as that of the tough-brittle transition process; its intensity obviously decreases by increasing the hydrosoluble content, which lowers the brittle strength of the material as shown before.

The maximum in the energy–temperature curves in the α-transition range is very broad and frequency dependent. It has not been possible to determine its activation energy because only the left-hand side of the maximum could be measured by the low-speed tests. In any case, the determination of the activation energy of this maximum should be strongly affected by the heat build-up during the test.

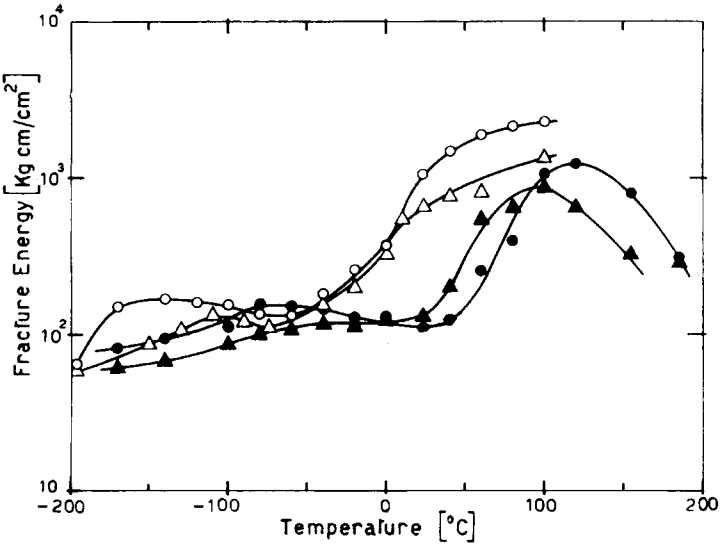

Fig. 19. Dependence of fracture energy on temperature and strain rate for samples A and E. $\dot{\epsilon} = 230$ sec^{-1}: (●) sample A; (▲) sample E. $\dot{\epsilon} = 5.5 \times 10^{-3}$ sec^{-1}: (○) sample A; (△) sample E.

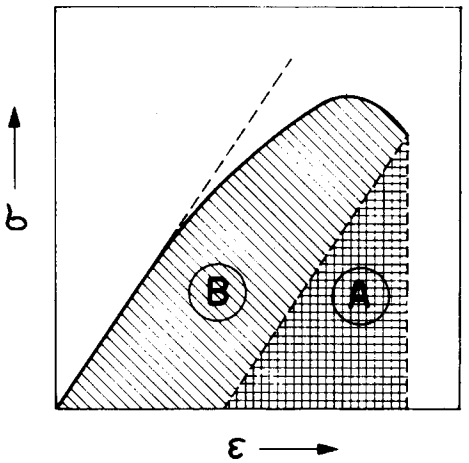

Fig. 20. Example of approximate method used to estimate elastic and plastic contributions to the total fracture energy. Area A roughly represents the elastic stored energy and area B, the plastic contribution.

The hydrosoluble content lowers the intensity of the maximum; but, inexplicably, the position on the temperature scale is shifted toward lower temperatures only for the high-speed tensile tests.

As pointed out before, the elastic energy stored and the energy dissipated through plastic deformations vary in different ways with temperature; therefore, the contributions of these two energies to the cumulative fracture

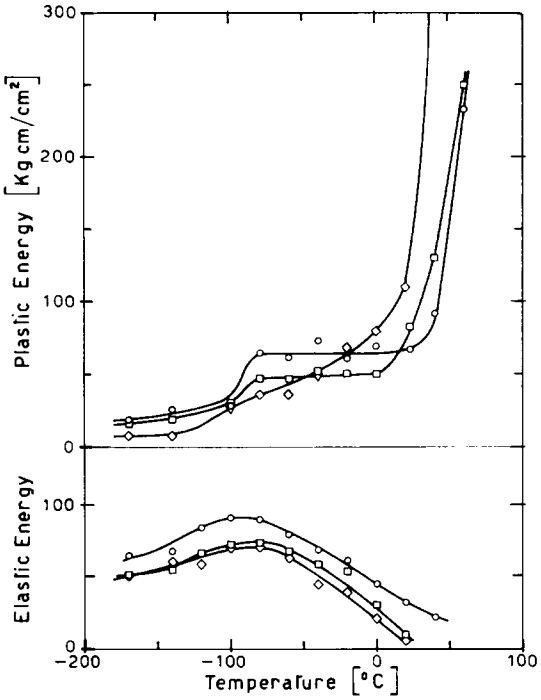

Fig. 21. Plot of elastic and plastic contributions to the total fracture energy vs. temperature for sample A (O), sample C (□), and sample E (◇).

energy were calculated from the stress–strain curves by means of a rough approximation method illustrated in Figure 20. The results obtained for tests carried out at $\dot{\epsilon} = 230\ \text{sec}^{-1}$ are plotted against the temperature for samples A, C, and E in Figure 21. The stored energy reaches a maximum at the tough-brittle transition temperature, then decreases monotonically with increasing temperature. This behavior is mainly determined by the decrease in yield strength and modulus, while the behavior at the lowest temperatures should be related to the maximum attainable strain, which is in turn determined by the cut-off level of the brittle strength.

The plastic energy is very low at temperatures below the tough-brittle transition temperature; then it increases and reaches a plateau in the plasto-elastic range; finally it increases suddenly in the α-transition range.

In the γ -transition zone, an inflection point is evident; it lies for sample A at about $-95°C$; such a temperature can be calculated also from the γ-activation energy for a frequency equal to $1/t_R$ (where t_R is the rupture time). The temperature of this inflexion point depends on the hydrosoluble content in the same way as T_γ obtained from dynamic-mechanical data (see Fig. 22). This result, like the one obtained from the modulus, indicates that the γ-relaxation process influences the plastic deformation energy even below the tough-brittle transition temperature.

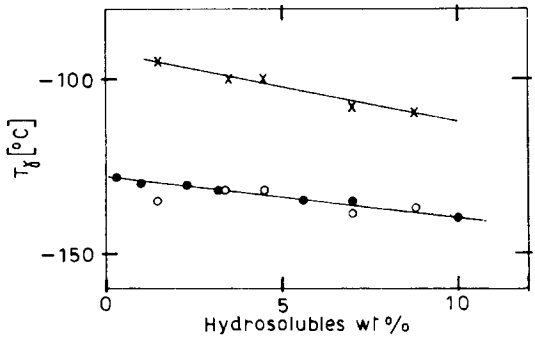

Fig. 22. Influence of hydrosoluble content on T_γ from dynamic-mechanical experiments: (O) this work; (●) ref. 6; (x) from plastic energy–T curves.

Izod Impact Strength

The Izod impact strength is reported in Figure 23 on a three-dimensional plot against temperature and hydrosoluble content. This shows that the impact strength increases slowly from −120°C to room temperature and that a sharp increase occurs only in the α-transition range. This trend is displaced toward lower temperatures by increasing the hydrosoluble content, that is, by decreasing the glass transition temperature.

For Izod impact strengths lower than 15 kg-cm/cm, all the autographic recorded curves, plotted in Figure 24 for sample E, show an apparent brittle behavior, since all the energy is used for crack initiation.[39,40] Only the curve at 40°C shows evidence that a deformation, at the tip of the notch occurs. These results show no appreciable influence of the γ-relaxation process on the Izod impact properties, as found previously in the case of tensile impact. At the same time, there is no evidence of any correlation between the β-relaxation process and the Izod impact strength, even in the case of sample E, which has the highest hydrosoluble content.

However, the morphology of the fracture surfaces, studied by electron scanning microscopy, always shows a plastic deformation of the specimens near the notch line (see Figs. 25, 26, and 27). In all cases, a point, from which the explosive crack has started, is clearly evident. It must be noted that the distance between the notch line and this point increases with the temperature, and so does the area interested by the plastic deformation.

Consequently at higher temperatures, a larger plastic flow is allowed, while, at the same time, the maximum load increases with temperature. This behavior is to be expected, since the radius of the notch increases with the amount of yielded material near the notch, bringing about a decrease in the stress concentration factor. However, the general failure behavior of the material for the Izod test is always apparently brittle, since only a small volume is involved in the plastic deformation.

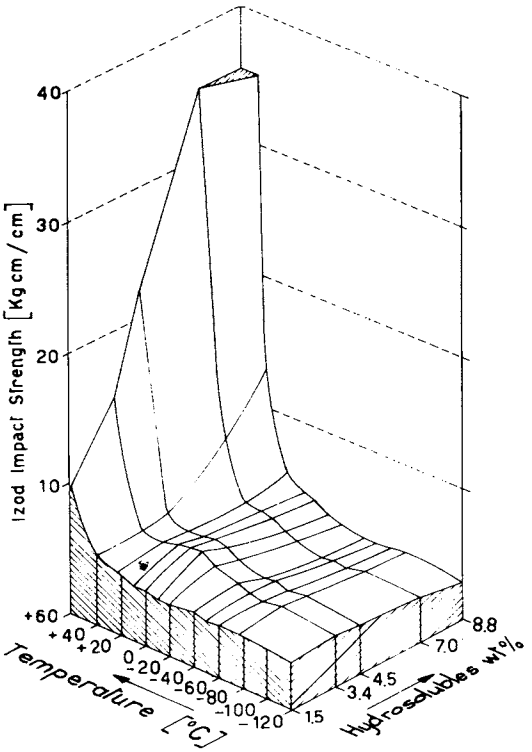

Fig. 23. Three-dimensional plot of Izod impact strength vs. temperature and hydrosoluble content.

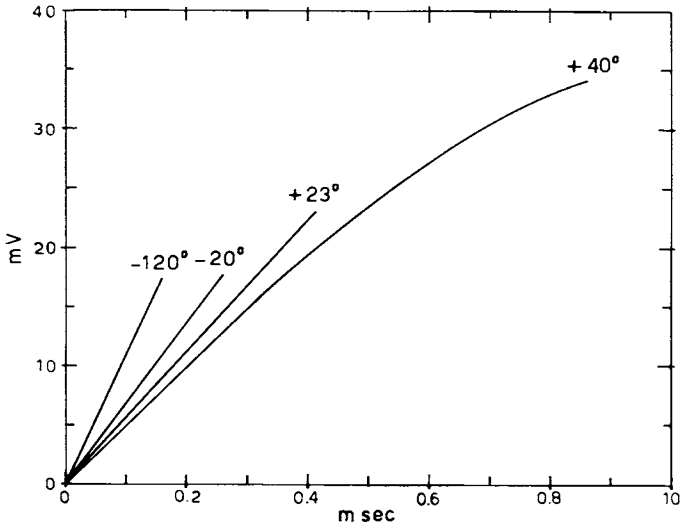

Fig. 24. Izod stress-time curves for sample E at different temperatures.

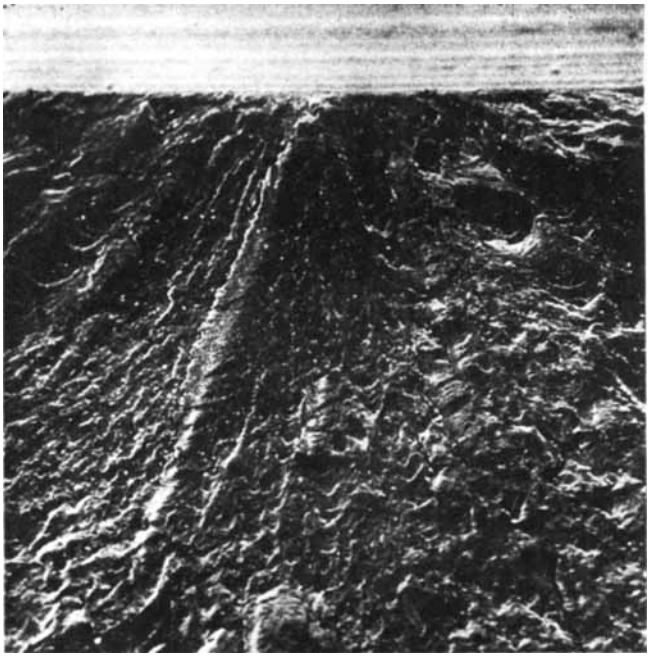

Fig. 25. Electron scanning micrograph (× 55) of fracture surface of a notched Izod specimen of sample E, broken at −120°C (see Fig. 24). White area is the notch surface.

The difference between the autographic curves obtained by the Izod (Fig. 9) and tensile impact test (Fig. 5) at temperatures higher than the tough-brittle transition temperature can be explained on the same basis.

It is well known[40–43] that the yield phenomenon in the Izod test is obscured by the geometry of the specimen, the mechanical arrangement of the test, and the shape of the notch, which has a drastic influence on the results of this test. The ASTM notch, for example, concentrates the stress in a very small volume of the material, and for this reason there is very little chance for large plastic deformation to occur. With other kinds of notches, the tough-brittle transition could be shifted toward lower or higher temperatures.[44] Some interesting results can also be obtained by considering the ratio in mV/msec derived from the recorded impact curves. In the present case, this quantity is a measure of the rigidity, which is proportional to a tangent modulus at low temperatures and, near T_α, to a secant modulus.

The mV/msec ratio is plotted in Figure 10 against the temperature for samples A, C, and E. The shape of these curves is like that of the moduli curves obtained from other kinds of experiments; the steps corresponding to T_γ and T_α are clearly evident, and the influence of hydrosolubles is similar to that observed for the moduli curves (see Figs. 1, 2, and 8).

Thus, in the case of the Izod impact test, it can be pointed out that, although some restrictive considerations should be applied to the energy

Fig. 26. Electron-scanning micrograph (× 55) of fracture surface of a notched Izod specimen of sample E, broken at −20°C (see Fig. 24). White area is the notch surface.

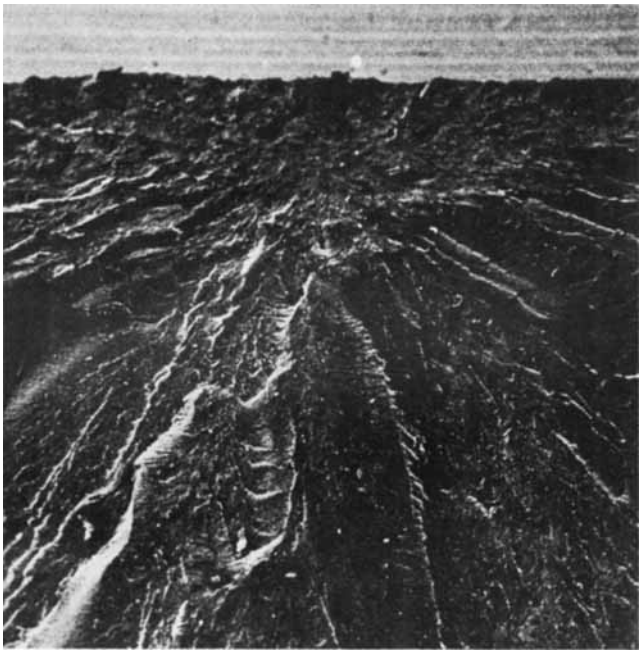

Fig. 27. Electron-scanning micrograph (× 55) of fracture surface of a notched Izod specimen of sample E, broken at 23°C (see Fig. 24). White area is the notch surface.

values, we are able by means of the autographic method to define a parameter whose relationship with moduli obtained by conventional method is very good.

CONCLUSION

The results obtained during this extensive investigation on the mechanical properties of nylon 6 (polycaprolactam) show that very useful information of structure–properties relationships of polymeric materials and on the controversial problem of the prediction of the ultimate and impact properties from dynamic-mechanical data can be gained.

As far as tensile modulus, "rigidity" from Izod test, and yield properties are concerned, the relationship is straightforward; these parameters can be related to well-defined relaxation processes, revealed by dynamic-mechanical measurements, according to the findings of other authors for different polymers.

In particular, it has been shown, by low-temperature measurements, that the γ-relaxation process, together with the α-process, contributes to the yielding behavior of polycaprolactam. The influence of strain rate and temperature on the tensile properties led us to consider the tough-brittle transition temperature from a new point of view; its activation energy has been related to molecular relaxation processes which determine the dependence of yield strength on temperature and on strain rate. It should be pointed out that its location on the temperature scale is nevertheless fixed by the value of the brittle strength σ_B, i.e., from defect loci concentration of test specimens. Our results indicate that tentative approaches of correlating dynamic-mechanical loss maxima and impact properties can lead to results not always reliable; the relationships are in fact strongly dependent on the mechanical aspects of test used, which tend to mask the viscoelastic contribution to the failure process. This has been shown either by properly handling mechanical data, for example, by dividing the total breaking energy into elastic and plastic contributions, or by using complementary investigation methods, such as autographic recording technique for the Izod test and observation of the fracture surfaces by electron-scanning microscopy.

As far as nylon 6 is concerned, a further insight into the structure–property relationships has been achieved by investigating the influence of hydrosoluble products on the dynamic-mechanical and mechanical properties.

The hydrosolubles were found to influence, through the well-known modification of the intermolecular hydrogen bonds, the dynamic-mechanical, the mechanical, and the impact properties in lowering T_α and T_γ; the tough-brittle transition temperature is an exception since it increases, because σ_B value is decreased in their presence. No appreciable influence of the β-relaxation process on mechanical and, in particular, on the ultimate properties has been noted, even though the β-dynamic-mechanical relaxa-

tion process is strongly affected by the hydrosoluble content. Such a result indicates that not all of the relaxation processes influence the engineering properties of materials.

In conclusion, relationships between dynamic-mechanical properties and the engineering properties of thermoplastic polymers should be more properly established by a comparison of the activation energies of the transition processes than by direct correlation relating the energy dissipated for a specific dynamic-mechanical transition to the fracture energy derived from tensile or Izod tests. We believe that for all polymers, the problem of relating the structure to mechanical properties can be adequately approached only by means of different techniques and test methods in a wide range of temperature and frequencies and through a careful analysis of the mechanical aspects of the test used.

We thank Prof. M. Pegoraro of the Polytechnic of Milan who read and commented the manuscript; Prof. G. Pezzin of the Montecatini-Edison Applied Research Laboratory, Porto Marghera, for helpful discussion and for the dynamic mechanical measurements carried out by the Brüel and Kjaer apparatus; Mr. P. Sangiovanni for the low-frequency dynamic-mechanical measurements; Mr. L. Colombaroli for the help in mechanical testing; and Mr. M. Solari who performed the microfractographies.

References

1. H. Oberst, *Kunststoffe*, **53**, 4 (1963).
2. L. Bohn, *Kunststoffe*, **53**, 826 (1963).
3. Y. Wada and T. Kasahara, *J. Appl. Polym. Sci.*, **11**, 1661 (1967).
4. R. F. Boyer, *Polym. Eng. Sci.*, **8**, 161 (1968).
5. P. I. Vincent, *Polymer*, **1**, 425 (1960).
6. G. Ajroldi, G. Vittadini, C. Garbuglio, and G. Convalle, *Chim. Ind.* (Milano), **49**, 265 (1967).
7. W. E. Hanford and R. M. Joyce, *J. Polym. Sci.*, **3**, 168 (1948).
8. G. M. Kline, *Analytical Chemistry of Polymers*, Part I, Interscience, New York, 1959.
9. T. Casiraghi, *Materie Plastiche*, **36**, 1053 (1970).
10. G. Convalle, Atti XV° Cong. Int. Mat. Plast., Torino, Sept. 1965, p. 79.
11. H. Oberst, in *Kunstoffe*, Vol. II, R. Nitsche and K. A. Wolf, Eds., Springer-Verlag, Berlin-Göttingen-Heidelberg, 1961.
12. L. E. Nielsen, *Mechanical Properties of Polymers*, Reinhold, New York, 1962.
13. T. H. Smith, *J. Polym. Sci.*, **20**, 89 (1956).
14. K. Schmieder and K. Wolf, *Kolloid-Z.*, **134**, 157 (1953).
15. A. H. Willbourn, *Trans. Faraday Soc.*, **54**, 717 (1958).
16. K. H. Illers, *Makromol. Chem.*, **38**, 168 (1960).
17. N. G. McCrum, B. E. Read, and G. Williams, *Anelastic and Dielectric Effects in Polymeric Solids*, Wiley, London, 1967, Chap. XII.
18. J. Kolarik and J. Janacek, *J. Polym. Sci. C*, **16**, 441 (1967).
19. C. Lanczos, *Applied Analysis*, Prentice-Hall, Englewood Cliffs, 1961.
20. E. Butta and C. Vannucchi, *Chim. Ind.* (Milano), **45**, 323 (1963).
21. M. L. Williams, R. F. Landel, and J. D Ferry, *J. Amer. Chem. Soc.*, **77**, 1301 (1955).
22. M. Takayanagi, *Mem. Pac. Eng. Kyushu Univ.*, **23** (1), 1 (1963).
23. K. Neki and M. Takayanagi, *Repts. Progr. Polymer Phys.* (Japan), **8**, (1965).
24. A. E. Woodward, J. M. Crissman, and J. A. Sauer, *J. Polym. Sci.*, **44**, 23 (1960).
25. M. Chatain and P. Dubois, *J. Appl. Polym. Sci.*, **6**, 70 (1962).

26. G. M. Bartenev and Yu. S. Zuyev, *Strength and Failure of Viscoelastic Materials*, Pergamon Press, London, 1968.
27. P. I. Vincent, in *Physics of Plastics*, P. D. Ritchie, Ed., Iliffe, London, 1965, Chap. II.
28. T. H. Smith, *J. Polym. Sci. A*, **1**, 3597 (1963).
29. J. A. Roetling, *Appl. Polym. Symposia*, **5**, 161 (1967).
30. R. E. Robertson, *J. Appl. Polym. Sci.*, **7**, 443 (1963).
31. J. C. Bauwens, C. Bauwens-Crowet, and G. Homès, *J. Polym. Sci. A-2*, **7**, 1745 (1969).
32. K. C. Rusch and R. H. Beck, *J. Macromol. Sci. B*, **3**, 365 (1969).
33. T. Ree and H. Eyring, in *Rheology*, F. R. Eirich, Ed., Academic Press, New York, 1958, Vol. II, Chap. III.
34. M. Reiner, *Deformation, Strain, and Flow*, Interscience, London, 1960, Chap. VI.
35. T. H. Smith, *J. Polym. Sci.*, **32**, 99 (1958).
36. W. Retting, *Rheol. Acta*, **8**, 259 (1969).
37. C. B. Bucknall, and D. G. Street, S. C. I. Monograph No. 26, 272, 1967.
38. K. C. Rusch, *J. Macromol. Sci.*, **B2**, 179 (1968).
39. W. E. Wolstenholme, in *High Speed Testing*, A. G. H. Dietz and F. R. Eirich, Ed., Vol. III, 1962, p. 85.
40. P. I. Vincent, *Plastics*, **27**, 116 (1962).
41. A. S. Tetelman and A. J. McEvily, *Fracture of Structural Materials*, Wiley, New York, 1957, Chap. VII.
42. E. Parker, *Brittle Behaviour of Engineering Structures*, Wiley, New York, 1957.
43. F. R. Eirich, *Appl. Polym. Symposia*, **1**, 271 (1965).
44. D. R. Reid and R. A. Horsley, *Brit. Plast.*, **32**, 156 (1959).

Received Febuary 4, 1971